Sintered Cathodes for All-Solid-State Structural Lithium-Ion Batteries

Will Huddleston[1], Frederick Dynys[2], Alp Sehirlioglu[1]

[1]Case Western Reserve University, Dept. Materials Science and Engineering, Cleveland, OH 44106, USA
[2]NASA Glenn Research Center, Cleveland, OH 44135, USA

Objective

- Characterize processing-structure-property relationships in cathode materials for optimized sintering conditions, structural and chemical stability, and microstructural development for all-solid-state structural lithium-ion batteries.
- Evaluate mechanical and electrical performance through ring-on-ring mechanical testing and impedance spectroscopy.

Motivation

- Achieve systems level weight savings in aerospace applications by providing multifunctional load bearing energy storage for all-electric or hybrid-electric propulsion systems.
- Improve upon the safety and reliability of energy storage systems by transitioning from liquid electrolytes to inherently safe all-solid-state battery configurations.

Background

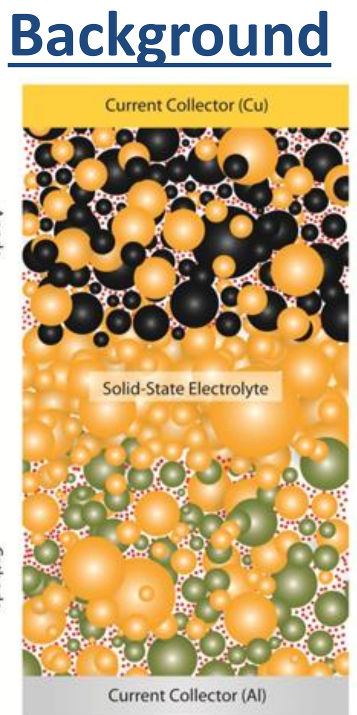

Figure 1: All-solid-state lithium-ion battery.[1]

- Secondary (rechargeable) all-solid-state lithium-ion batteries store electrical energy as chemical potential energy.
- Anode – receives Li^+ during charging, releases Li^+ during discharge.
- Electrolyte – allows facile diffusion of Li^+ between composite electrodes, negligible electronic conductivity prevents leakage.
- Cathode – releases Li^+ during charging, receives Li^+ during discharge.
- Typical composite electrodes are composed of active material, electrolyte, and a electronically conductive additive phase.
- Multifunctional structural batteries provide energy storage and load-bearing performance to achieve overall weight reduction.

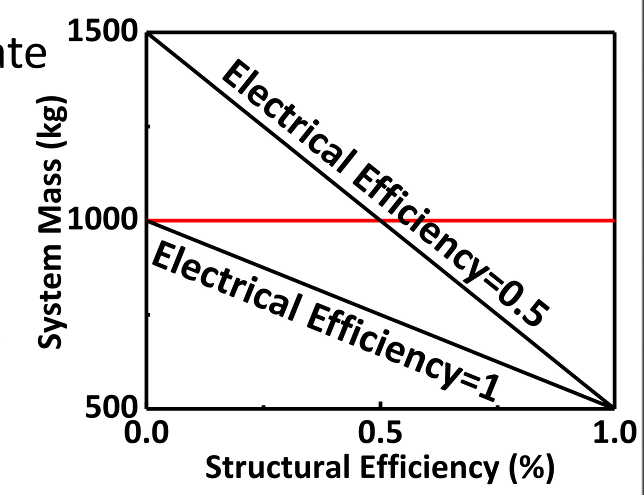

Figure 2: Schematic plot for system design to achieve overall weight savings.[2]

[1] http://smeng.ucsd.edu/supercapacitors/ [2]After L. E. Asp, "Multifunctional composite materials for energy storage in structural load paths"

Materials

- Commercially available cathode active material $Li(Ni_{0.33}Mn_{0.33}Co_{0.33})O_2$ (NMC).
- As-received agglomerates ball milled to liberate particles, reduce and homogenize particle size distribution.

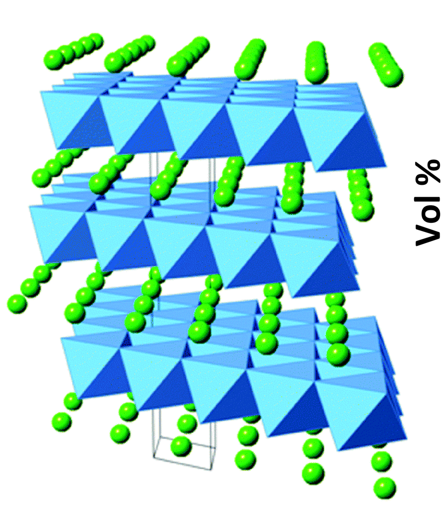

Figure 3: Layered structure displaying transition metal octahedrons and lithium layers.[3]

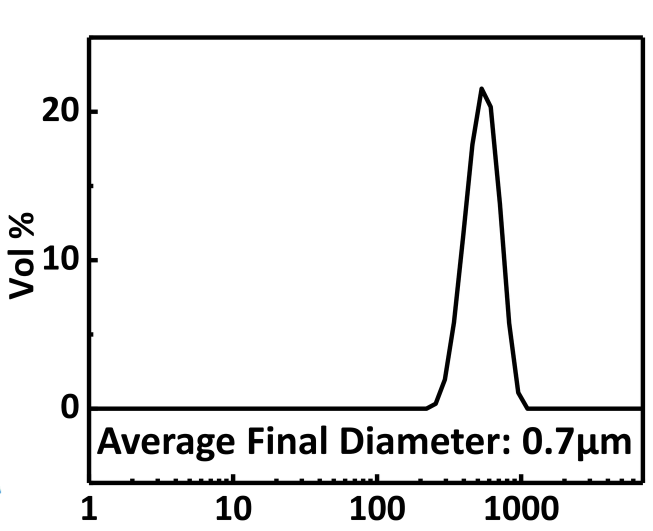

Figure 4: volume fraction particle size distribution of milled NMC from dynamic light scattering.

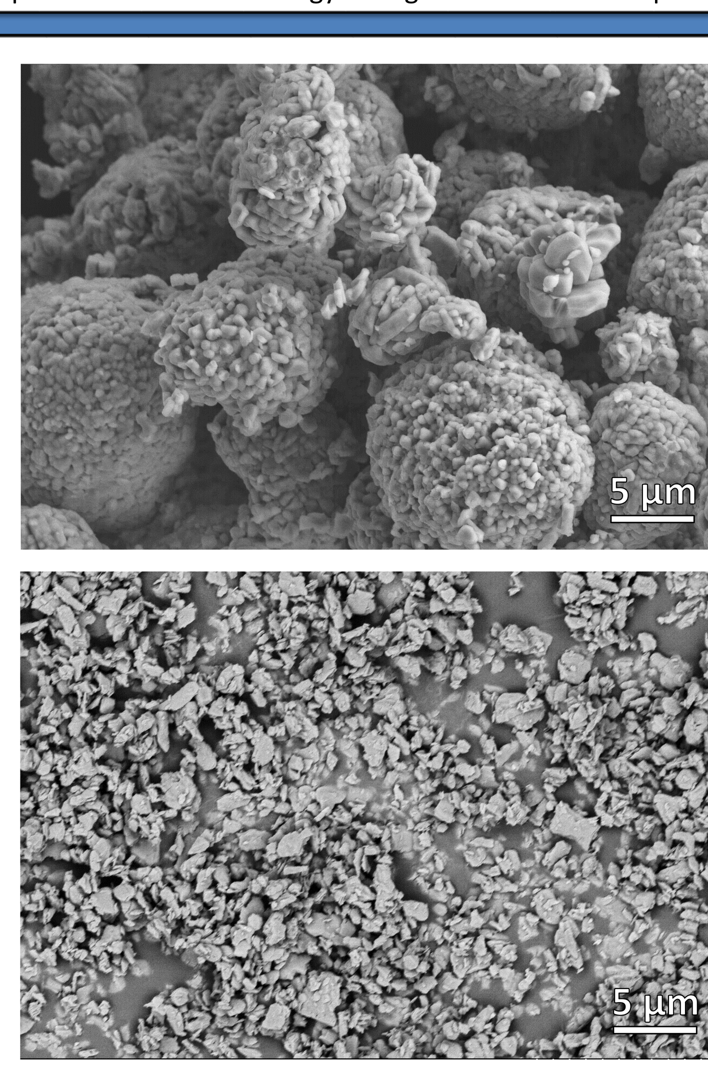

Figure 5: Top: NMC agglomerates. Bottom: NMC after 20hrs of ball milling.

3: "Lithium and sodium battery cathode materials: computational insights into voltage, diffusion, and nanostructural properties" M. Islam and C. Fisher. *Chem. Soc. Rev.*, 2014, 43, 185-204

Structural and Chemical Stability

Table 1: ICP data for various processing states and sintering conditions. AR – as received, M – milled.

Wt. %	AR	M	1000°C-1Hr	1050°C-1Hr	1100°C-1Hr
Li	7.2	7.2	7.1	7.1	7.0
Ni	20.9	20.7	21.4	20.8	21.0
Mn	19.0	18.8	19.5	19.0	19.1
Co	19.9	19.7	20.5	20.0	20.0

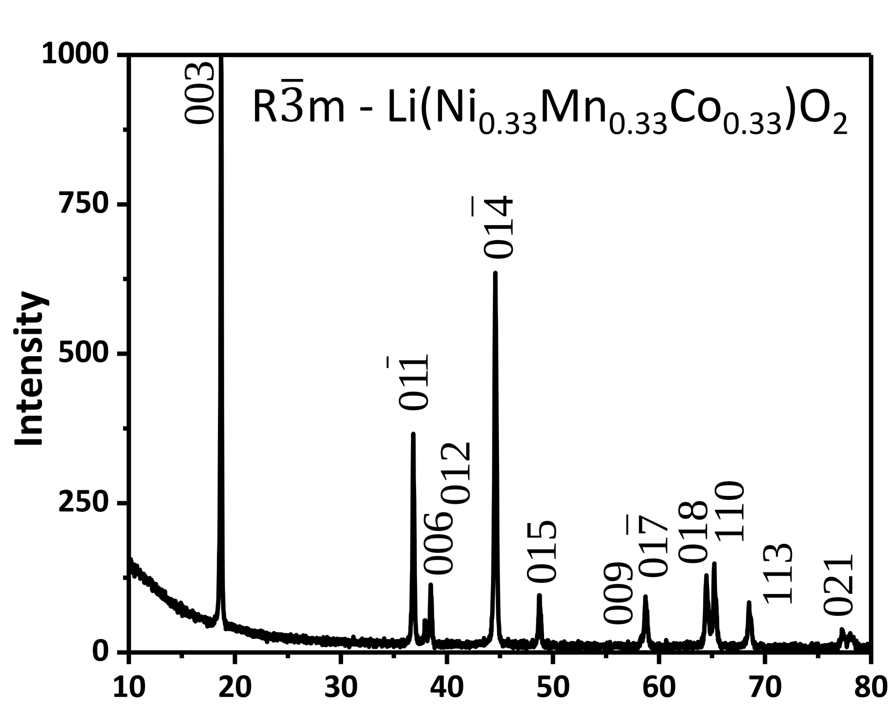

Figure 6: Typical XRD pattern for layered $R\bar{3}m$ $Li(Ni_{0.33}Mn_{0.33}Co_{0.33})O_2$.

- Li, Ni, Mn, & Co composition controlled with use of sacrificial powder bed.
- ICP indicates 3% lithium volatilization at highest sintering temperature and is within instrument uncertainty.
- XRD patterns of rhombohedral layered structure remain unchanged across processing temperature range from 1000°C to 1100°C.

Acknowledgements: Ben Kowalski and Kevin Pachuta at Case Western Reserve University and, Jon Mackey, Dan Gorican, Rick Rogers, and Terry McCue at NASA Glenn Research Center

Densification and Coarsening

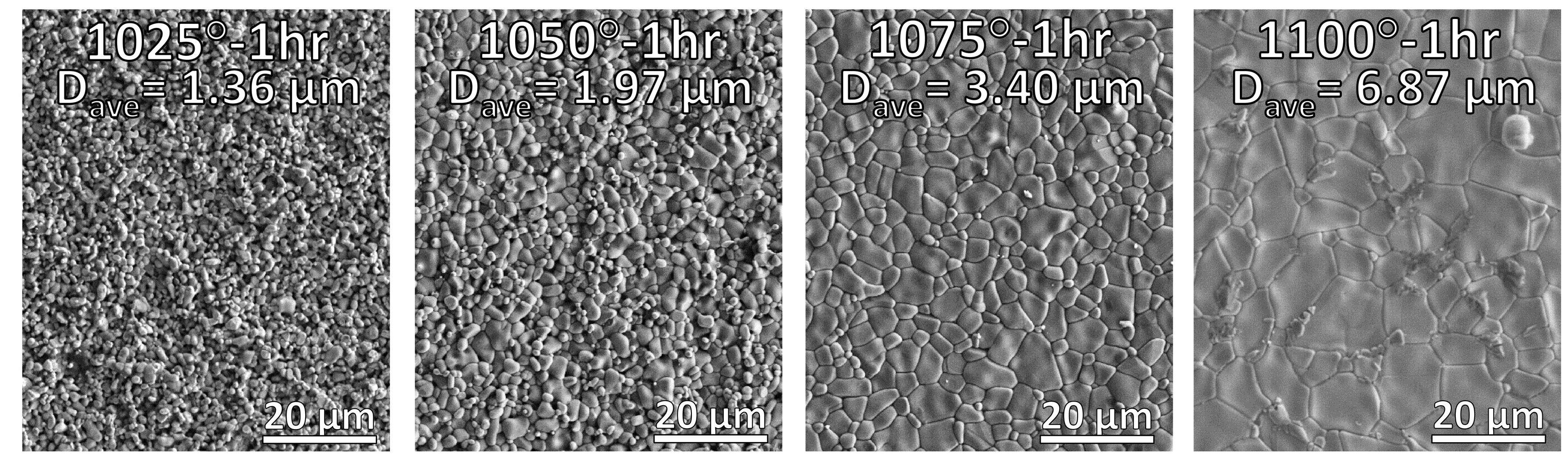

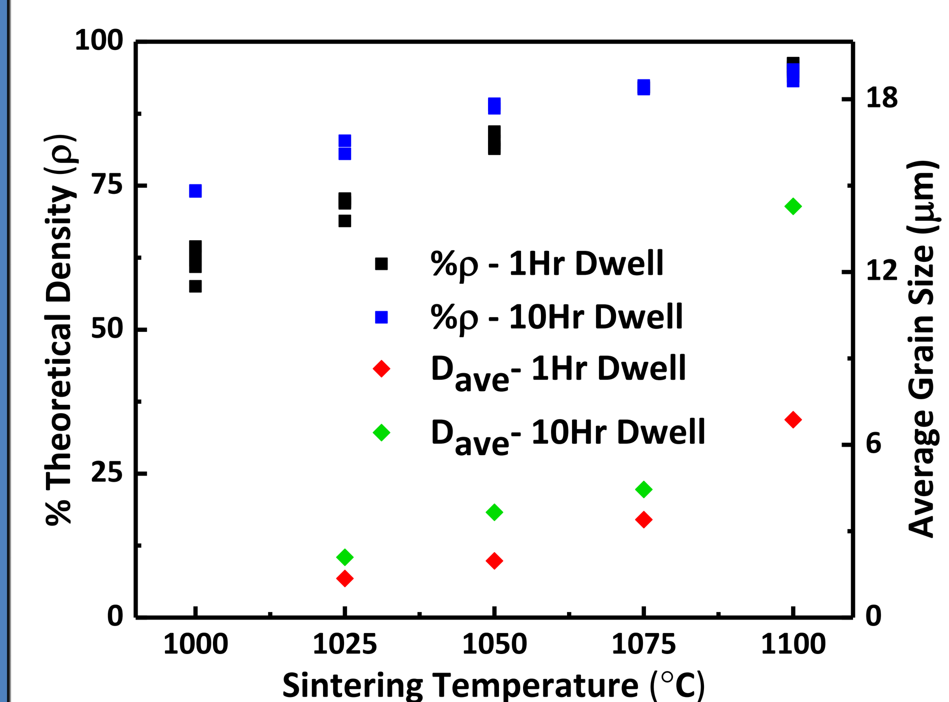

Figure 7: Above, sintered microstructures for samples processed with increasing sintering temperature. Average grain size is tabulated beneath each micrograph.

Figure 8: Left, plot displaying average percentage of theoretical density and average grain size for samples for all sintering temperatures.

- >90% theoretical density reached at 1075°C and above.
- Significant grain growth occurs at sintering temperatures above 1075°C.

Mechanical Performance

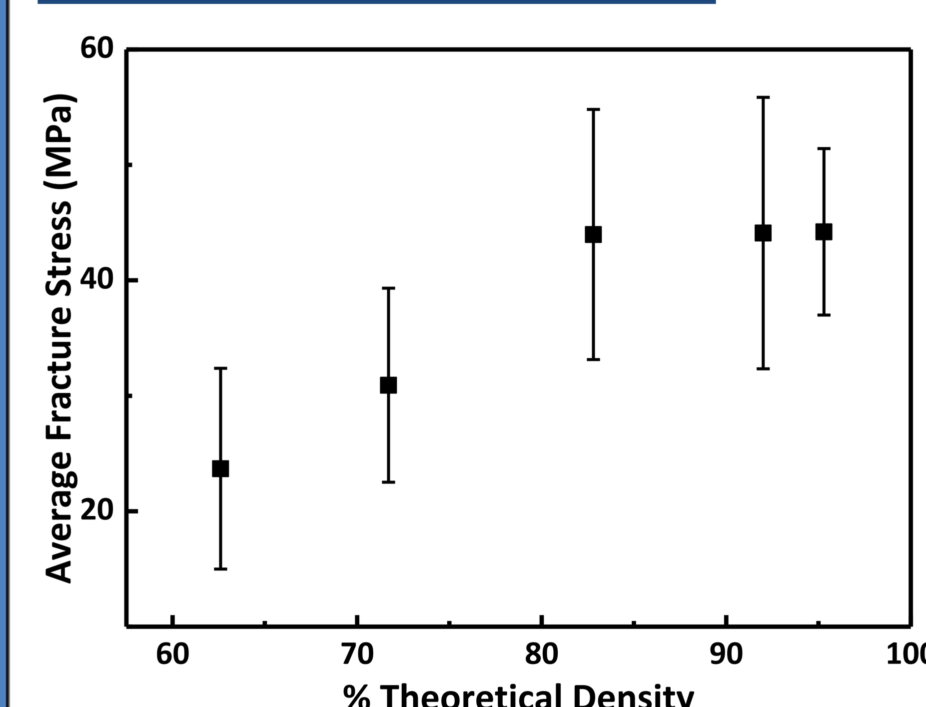

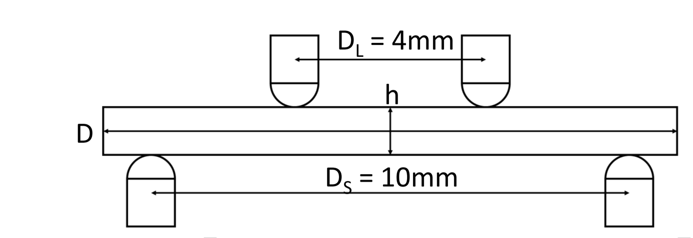

$$\sigma_f = \frac{3F}{2\pi h^2}\left[(1-\nu)\frac{(D_s^2 - D_L^2)}{2D^2} + (1+\nu)\ln\frac{D_s}{D_L}\right]$$

σ_f – fracture stress (MPa)
h – specimen thickness (mm)
D – specimen diam. (mm)
D_S – support ring diam. (mm)
F – load at failure (N)
D_L – load ring diam. (mm)
ν – Poisson's ratio

Figure 9: Left: ring-on-ring mechanical fracture stress as a function of percent theoretical density.

Figure 10: Above: ring-on-ring mechanical testing and analysis performed according to ASTM C1499-15.

- Mechanical fracture stress correlates with densities greater than 83% of theoretical density. Weibull analysis indicates reliability increases with reduction in porosity.

Electrical Performance

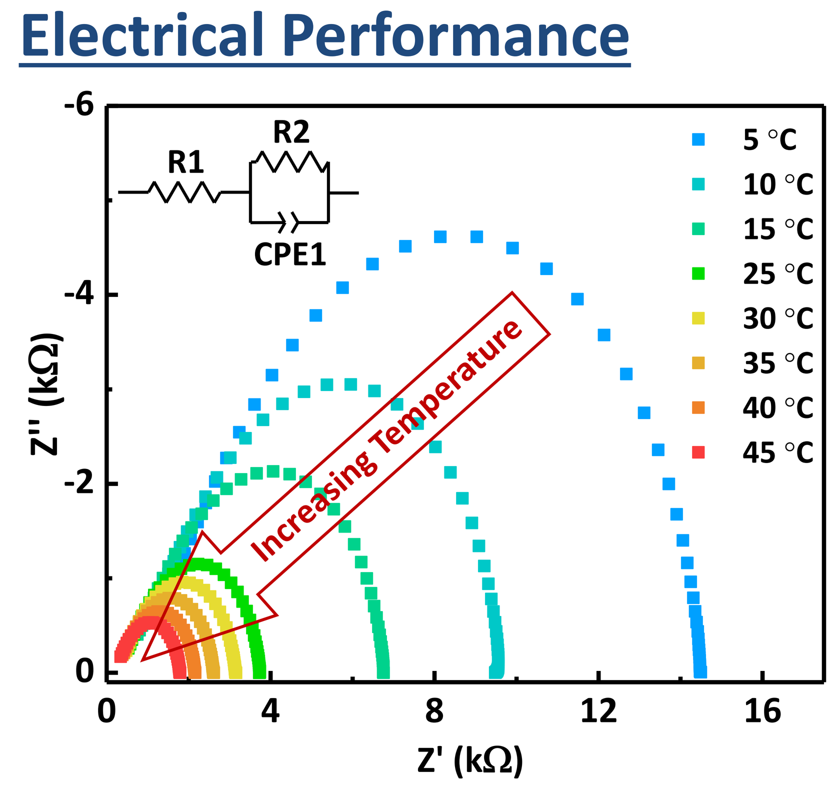

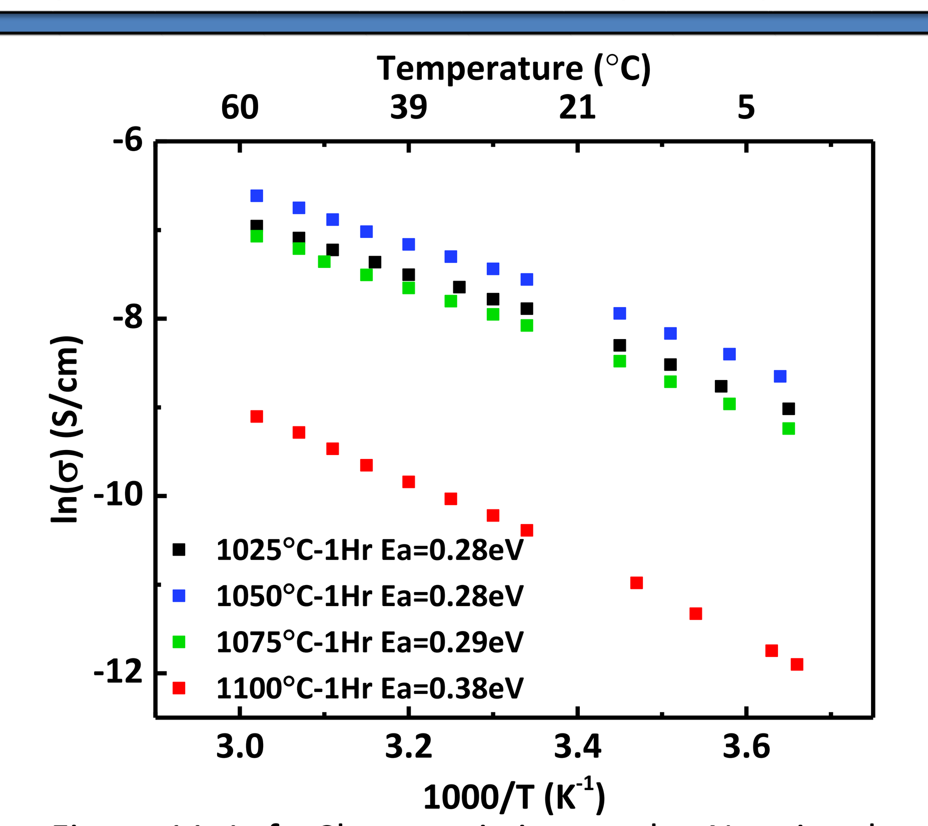

Figure 11: Left: Characteristic complex Nyquist plot for sintered cathode samples and equivalent circuit model used in impedance spectroscopy curve fitting.

Figure 12: Right: electronic conductivity as a function of inverse temperature. Activation energies were calculated from linear fit Arrhenius slopes.

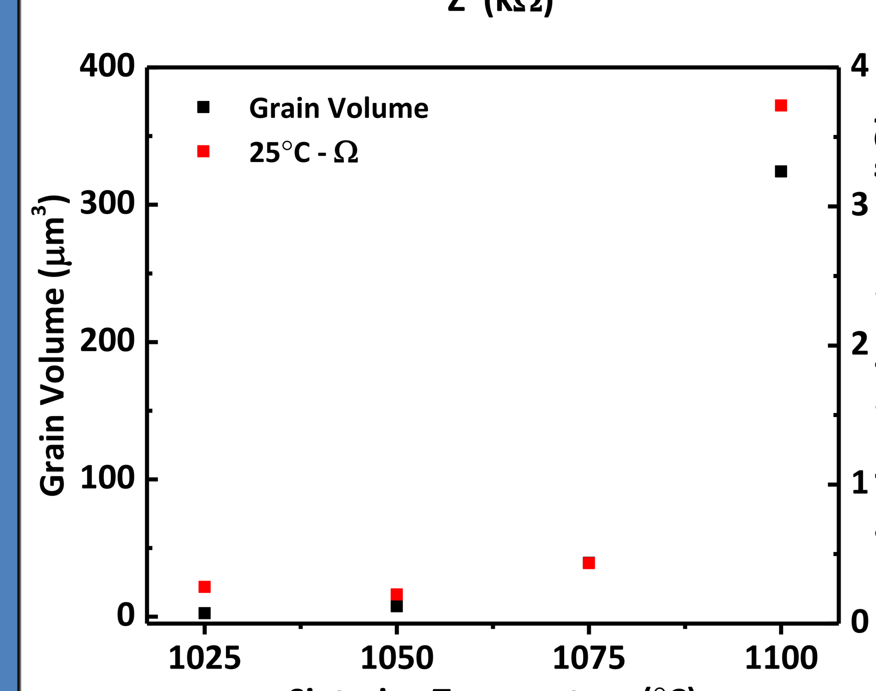

Figure 13: Below: plot demonstrating direct correlation between grain volume and electrical resistance.

- Grain growth correlates with increase in overall resistance, indicating grain boundary conduction as the dominant mechanism for electrical conductivity.

Conclusions:

- Microstructural development of $Li(Ni_{0.33}Mn_{0.33}Co_{0.33})O_2$ has been studied in relation to its mechanical and electrical properties.
- Greater than 90% density can be achieved when sintering at and above 1075°C.
- Fracture stress correlates with sample density and is maximized near 45MPa. Mechanical performance requires composite infiltration to overcome brittle fracture failure before structural application may be realized.
- At 1100°C, grain coarsening leads to higher electrical resistivity, indicating conduction dominated by grain boundaries.